Impact of Structural Polymorphs on Charge Collection and Non-Geminate Recombination in Organic Photovoltaic Devices

Panagiotis E. Keivanidis [1], Jafar I. Khan [2], Leon Katzenmeier [2], Zhipeng Kan [2], Saurav Limbu [3], Marios Constantinou [1], Eirini Lariou [4], Georgios Constantinides [1], Sophia Hayes [4], Ji-Seon Kim [3], Frédéric Laquai [2*]*

[1] Department of Mechanical Engineering and Materials Science and Engineering, Cyprus University of Technology, 45 Kitiou Kyprianou str., Limassol 3041, Cyprus

[2] King Abdullah University of Science and Technology (KAUST), KAUST Solar Center (KSC), Physical Sciences and Engineering Division (PSE), Thuwal 23955-6900, Kingdom of Saudi Arabia

[3] Department of Physics and Centre for Plastic Electronics, Imperial College London, London SW7 2AZ, United Kingdom

[4] University of Cyprus, Department of Chemistry, Cyprus

AUTHOR INFORMATION

Corresponding Author

* p.keivanidis@cut.ac.cy; frederic.laquai@kaust.edu.sa

ABSTRACT: The formation of different types of structural polymorphs of poly(3-hexyl-thiophene) (P3HT) affects the performance of organic photovoltaic (OPV) devices that use thermally-annealed P3HT:PCBM[60] blend films as photoactive layer. Here it is demonstrated that, when densely-packed and non-densely packed P3HT polymorphs co-exist in the P3HT:PCBM[60] layer, non-geminate charge recombination is fast; however, in a device non-geminate recombination is effectively overruled by efficient and fast charge carrier extraction. In stark contrast, when only a less-densely packed P3HT polymorph is present in the blend, non-geminate charge recombination losses are less pronounced, and the charge carrier extraction efficiency is lower. The antagonistic non-geminate charge recombination and charge carrier extraction processes in these systems are monitored by time-delayed-collection field (TDCF) and ultrafast transient absorption (TA) experiments. Furthermore, resonance Raman spectroscopy reveals that in the absence of the densely-packed P3HT polymorph, the energetic disorder present in the P3HT:PCBM[60] blend is higher. High-resolution atomic force microscopy imaging further identifies pronounced differences in the layer morphology when the polymorph distribution varies between unimodal and bimodal. These results indicate that less-densely packed P3HT polymorphs increase disorder and impede charge collection, leading to a reduction of the device fill factor.

Introduction

In the past twenty years, the use of electronically-active (semiconducting) organic materials for charge photogeneration has sparkled an intense research activity around the development of organic photovoltaic (OPV) devices. [1-3] Bulk heterojunction OPV composite films comprise an electron-donating matrix blended with small molecular or polymeric electron-acceptors, in turn creating a heterojunction for charge separation and interpenetrating networks that facilitate charge transport towards the respective charge-collecting contacts of the OPV device. [4, 5] Following the light absorption by the OPV photoactive layer, the crucial step determining charge photogeneration is the dissociation of the primary photoexcitations, namely neutral excited states (excitons), at the donor/acceptor interface (the heterojunction).[6] Equally important is the efficiency of the interfacial charge-separation step, which determines the escape of charges from their mutual Coulomb attraction and conversion of charge-transfer states (geminate charge pairs) to free charge carriers, that can be extracted as photocurrent; free carriers are produced when the antagonistic process of geminate charge pair recombination is suppressed.[7, 8] Furthermore, when the carrier mobility of the blend is optimized, a swift charge carrier extraction at the device electrodes is ensured with minimum dwell time of charges in the active layer, reducing the carrier loss due to non-geminate recombination which competes with carrier extraction.[9] Clearly, all aforementioned (photo)physical processes are strongly influenced by the OPV layer microstructure and it is challenging to achieve a balance of structural motifs that simultaneously optimizes all the individual process. As such, the preparation of OPV photoactive layers by wet-lab processing techniques is a perplexing task that relies on smart protocols and empiric optimization of the layer microstructure. Phase coarsening via thermal annealing,[10] use of poly(3-hexyl-thiophene) (P3HT) with different molecular weight,[11] composition dependence, [12] use of solvents/co-solvents with different boiling points, [13] use of additives and controlled plasticization,[14] are some of the techniques

that have been applied in an effort to gain control over the microstructure of OPV layers and to maximize excited state dissociation, full charge separation, and charge carrier extraction. However, an important aspect that yet has remained unexplored is the impact of the presence of different polymer polymorphs [15, 16] on the competition between charge carrier extraction and non-geminate geminate recombination losses. Particularly for the case of P3HT, previous temperature-dependent fluorescence studies have inferred the presence of different P3HT polymorphs in single-component P3HT films.[17] Yet, it remains unclear whether certain types of polymorphs are required to enhance the collection of photo-generated charge carriers at the device electrodes. It is imperative that this missing information can be provided to elucidate the role of material polymorphism on the performance of OPV devices.

In this contribution, we shed light on the role of polymorph structures on the competition between non-geminate charge recombination and charge extraction in operating OPV devices. In our work, we study the archetypical OPV system P3HT:PCBM[60] [18] to directly address the impact of P3HT polymorphism on device performance. Two well-defined polymorph structures of the P3HT polymer matrix are employed, and their effect on the power conversion efficiency (PCE) of P3HT:PCBM[60] devices is interrogated. For the first time, our study unveils how a specific distribution of structural polymorphs present in the hole-transporting polymeric matrix of P3HT can facilitate the charge collection efficiency, despite the occurrence of significant non-geminate recombination losses that take place in the photoactive layer.

In our study we focus on OPV devices with two types of P3HT:PCBM[60] photoactive layers, for which the polymorph distribution of the P3HT matrix is tuned by varying the number-averaged molecular weight (M_n) of the P3HT polymer matrix. Two P3HT derivatives with different M_n values are examined: a high-M_n P3HT derivative with M_n= 29.6 kDa (RR= 95.7%) and a low-M_n P3HT derivative with M_n=18.3 kDa (RR=95.2%). We have recently demonstrated that profound differences exist in the P3HT polymorph distribution present in

thermally-annealed P3HT:PCBM[60] blends of these two derivatives. [19] More precisely, a bimodal distribution of P3HT polymorphs was identified in the low-M_n P3HT-based OPV blend indicating the co-existence of a 'densely-packed' and a 'non-densely packed' P3HT polymorph. Instead, only the non-densely packed P3HT polymorph was identified in the high-M_n P3HT-based OPV blend of P3HT:PCBM[60]. Here we further demonstrate that, when the densely-packed P3HT polymorph is present in the P3HT:PCBM[60] photoactive layer, the charge collection efficiency is maximized, leading to a fill factor (FF) as high as 60%, despite fast non-geminate charge recombination.

The specificity of efficient charge carrier collection in the presence of a particular P3HT polymorph in the microstructure of the P3HT:PCBM[60] layer resolves the major issue of free carrier losses, that is, non-geminate recombination competing with charge carrier extraction, which hitherto remain convoluted. More importantly, our findings offer useful guidelines for the accurate engineering of next-generation OPV layers by introducing polymorphism as a tool to improve charge collection and to increase device performance.

We combine resonant Raman and ultrafast transient absorption (TA) spectroscopic characterization of P3HT:PCBM[60] blend films with high-resolution atomic force microscopy (AFM) imaging of the layers and electrical characterization of the corresponding P3HT:PCBM[60] OPV devices. The impact of the P3HT polymorph distribution on the energetic disorder of the P3HT:PCBM[60] blend film is assessed with Raman spectroscopy, while ultrafast TA measurements provide quantitative information on the processes of charge photogeneration and recombination. In addition to the obtained TA results, the effect of charge carrier collection on the overall device performance of the two systems studied herein is further explored by time-delayed collection field (TDCF) experiments.[20]

Results and Discussion

The fabrication of OPV devices with P3HT:PCBM[60] photoactive layers processed identically to those used as TA samples directly links the obtained TA results to the device performance of these systems. Table 1 presents a comparison of the figures-of-merit of the two types of OPV devices prepared with as-spun and thermally-annealed P3HT:PCBM[60] photoactive layers, when the two different M_n P3HT derivatives are used. A well-established device fabrication protocol was followed, and the reproducible character of the obtained results is adequately verified by their agreement with the previously performed systematic study of OPV devices developed by identical photoactive layers.[19] At present, 4 – 5 devices of each system were characterized, and Table 1 reports the mean value of each figure of merit accompanied by the corresponding standard deviation; namely the short-circuit current density (J_{SC}), the open-circuit voltage (V_{OC}), the fill factor (FF) and the power-conversion efficiency (PCE). The maximum PCE obtained is 2.3%, which is acceptable for conventional P3HT:PCBM[60] OPV cells [18] prior to the fine tuning of the P3HT:PCBM[60] photoactive layer composition, and without incorporating any charge carrier extracting interlayers in their device structure. Table 1 informs that the highest PCE is delivered by the low-M_n P3HT-based OPV cell after annealing, for which the averaged FF parameter reaches 60%.

Device type	J_{SC} (mA cm^{-2})	V_{OC} (mV)	FF (%)	PCE (%)
As-spun high-M_n	1.75 ± 0.03	809 ± 17	28.4 ± 0.6	0.4 ± 0.01
As-spun low-M_n	2.25 ± 0.08	698 ± 10	41 ± 2	0.65 ± 0.05
Annealed high-M_n	5.16 ± 0.17	564 ± 4	30.7 ± 1.1	0.89 ± 0.04
Annealed low-M_n	7.00 ± 0.10	545 ± 2	60 ± 0.8	2.3 ± 0.06

Table 1. Figures-of-merit for the P3HT:PCBM[60] 1:1 OPV devices investigated in this study.

Resonance Raman spectra (photoexcitation either at 488 nm or at 473 nm) were recorded [21] for as-spun and thermally-annealed P3HT:PCBM[60] photoactive layers prepared by both types

of P3HT matrices. Two vibrational modes associated with the thiophene ring within the main P3HT polymer chain were monitored. The C=C symmetric stretch mode centered at ~ 1445 cm^{-1} and the C-C stretch mode centered at ~ 1380 cm^{-1}. [22] Two sets of Raman measurements were performed for the P3HT:PCBM[60] layers; one for films deposited on glass/ITO/PEDOT:PSS substrates (semi-complete OPV device geometries), and another one for films prepared on plain quartz substrates. Regardless of the substrate type used, the Raman spectra (shown in Supporting Information, Figure S1) demonstrate that upon thermal treatment of the layers the Raman peak at 1445 cm^{-1} exhibits a ~ 5 cm^{-1} peak shift towards lower (Raman) wavenumbers, accompanied by a concomitant reduction in FWHM and an increase in the ratio of the C-C/C=C peak intensities. This observation is attributed to the minimization of energetic disorder in both types of P3HT:PCBM[60] photoactive layers after thermal annealing, due to the increased planarity of the P3HT backbone and the concomitant reduction of twists between thiophene monomers. Table 2 summarizes the C=C peak position and peak width of these samples. Interestingly, relative to the low-M_n annealed P3HT:PCBM[60] film, the high-M_n annealed P3HT:PCBM[60] film exhibits a larger FWHM of the C=C stretching mode, suggesting that despite the thermal processing applied, some energetic disorder persists, when the non-densely packed P3HT polymorphs dominate in the P3HT:PCBM[60] layers. Similar results are obtained for the thermally-annealed P3HT:PCBM[60] blends, when Raman measurements are performed down to a temperature of 50 K after photoexcitation at 473 nm (see Raman spectra and tabled centers and FWHM values of the C=C symmetric stretch mode shown in Supporting Information, Figure S2 and Table S1), however, the overall FWHM values of the C=C Raman peak are found to be increased. Both at room and at low temperatures, the use of the PEDOT:PSS interlayer results in reduction in the FWHM values of the C=C Raman peak (see in Supporting Information, Figure S3) most likely due to differences in the degree of vertical phase separation of the P3HT and PCBM[60] components of the blends. [22,

[23] However, the trends of the FWHM values for the high-M_n and low-M_n P3HT:PCBM[60] films after thermal annealing remain the same. As such, the Raman study shows that the content of energetic disorder in the studied P3HT:PCBM[60] layers is affected by the P3HT polymorph distribution in the layers but it is insensitive to the type of substrate supporting these layers. The results highlight the capability of Raman spectroscopy to probe energetic disorder in contactless photoactive layers. This straightforward spectroscopic approach is complementary to electrical device characterization techniques that directly quantify energetic discorder, *e.g.* by monitoring the temperature-dependence of charge carrier mobility. [24, 25] Such a detailed device characterization experiment could be further performed for verifying the findings of the herein presented Raman study, however it is beyond the scope of our present work.

System	C=C centre (cm^{-1})	C=C FWHM (cm^{-1})
As-spun high-M_n on glass/ITO/PEDOT:PSS substrate	1451.3 ± 0.7	39 ± 1
Annealed high-M_n on glass/ITO/PEDOT:PSS substrate	1448.5 ± 0.7	31 ± 1
As-spun low-M_n on glass/ITO/PEDOT:PSS substrates	1452.4 ± 0.7	39 ± 1
Annealed low-M_n on glass/ITO/PEDOT:PSS substrate	1447.9 ± 0.7	29 ± 1
As-spun high-M_n on quartz substrate	1454.1 ± 0.7	39 ± 1
Annealed high-M_n on quartz substrate	1448.5 ± 0.7	32 ± 1
As-spun low-M_n on quartz substrate	1453.2 ± 0.7	40 ± 1
Annealed low-M_n on quartz substrate	1448.5 ± 0.7	30 ± 1

Table 2. Overview of the room temperature Raman results obtained for the P3HT:PCBM[60] films investigated in this study following photoexcitation at 488 nm.

The surface topography of the two different photoactive layers is presented in **Figure 1**. High-resolution atomic force microscopy (AFM) imaging (100 × 100 nm) reveals that the surface texture of the low-M_n and the high-M_n P3HT-based P3HT:PCBM[60] films differs significantly when annealed at 140° C. The former exhibit elongated finger-like interdigitating

features (see Fig.1a), while the latter adapts a grape-like morphology (see Fig.1b), with lower aspect ratio features. Interestingly, this morphological discrepancy is less pronounced when AFM scans are made in a larger range, *e.g.* in 500 × 500 nm (see Fig.1c, d), demonstrating the necessity to perform high-resolution AFM scans for revealing subtle differences in the morphologies of OPV photoactive layers. The height distribution histogram profiles of both types of P3HT:PCBM[60] films (see Fig.1e, f) reveal that the surface of the low-M_n P3HT-based P3HT:PCBM[60] film is smoother, with a peak roughness of 7 nm in contrast to the peak roughness of the high-M_n P3HT-based P3HT:PCBM[60] film that was found to be 10 nm.

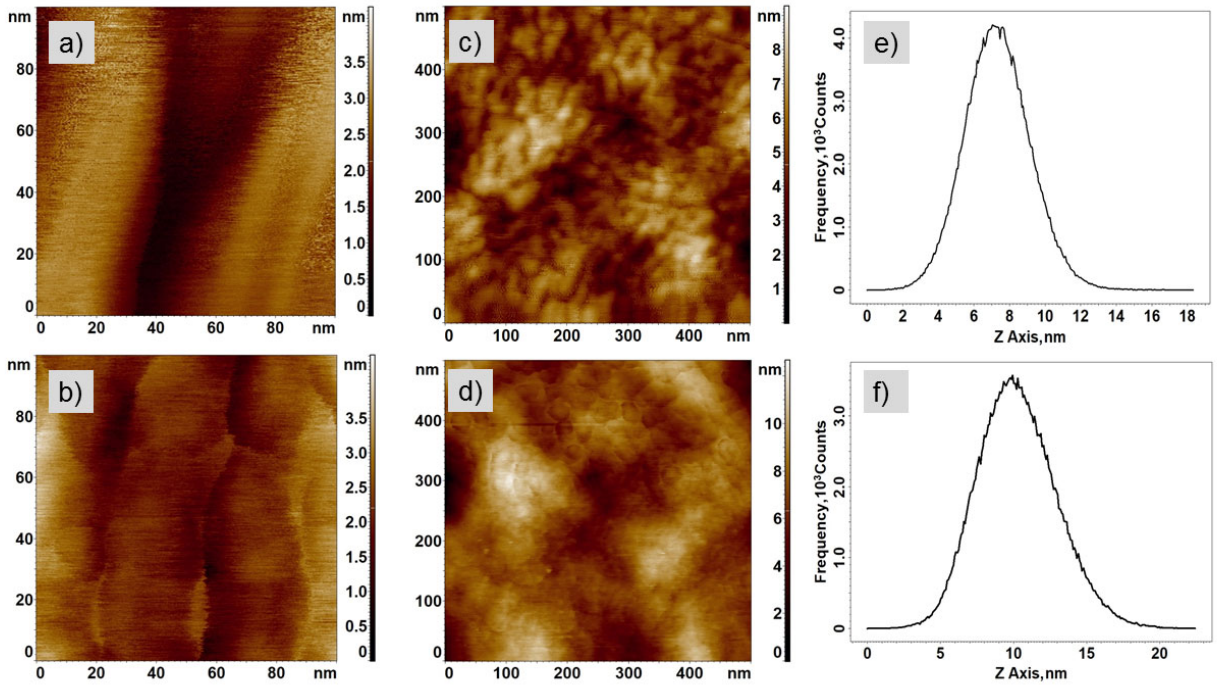

Figure 1. High-resolution (100 × 100 nm) AFM images of a) low-M_n P3HT-based and b) high-M_n P3HT-based P3HT:PCBM[60] films. Intermediate-resolution (500 × 500 nm) AFM images of c) low-M_n P3HT-based and d) high-M_n P3HT-based P3HT:PCBM[60] films. Height distribution histogram profiles of surface features detected in the AFM images of the e) low-M_n P3HT-based and f) high-M_n P3HT-based P3HT:PCBM[60] films. All histograms were built based on 5 × 5 μm AFM images. In all cases the P3HT:PCBM[60] films were developed on glass/ITO/PEDOT:PSS substrates and they were thermally annealed at 140° C.

Intrigued by the substantially different FFs found in the two types of annealed P3HT:PCBM[60] OPV devices (Table 1),[17] we performed TDCF experiments on the BHJ

systems. In the TDCF experiment the device is illuminated by a short laser pulse, while being kept at constant pre-bias voltage (V_{pre}). After a variable time delay t_d, a rectangular bias voltage (V_{coll}) with 1 μs pulse length is applied to extract (collect) all remaining free carriers from the device. The measured photocurrent response exhibits two current peaks, one following photoexcitation, and a second after application of the V_{coll} extraction pulse. Integration of the area below the two curves yields the quantity of charges generated by photoexcitation (Q_{pre}) and extracted before (with an applied V_{pre} bias), and during (Q_{col}) the application of the collection field, respectively (with an applied V_{coll} bias). The sum of Q_{pre} and Q_{col} equals the total number of generated charges Q_{tot}. Figure S4 in the Supporting Information section visualizes the TDCF experiment.

Figure 2 below presents the dependence of photocurrent generation on the laser fluence when the low-M_n (Fig.2a) and high-M_n (Fig.2b) P3HT-based OPV devices were photoexcited at 532 nm with a sub-ns laser pulse. For this experiment, the laser fluence was varied between 0.1 – 4.4 μJ cm^{-2}, the t_d was kept at 10 ns and the constant pre-bias voltage was set to V_{pre}= 0 Volts (*i.e.* short-circuit conditions). A power-law function $Q \propto I_{exc}^{\alpha}$ was applied to the datasets of Fig. 2 where Q corresponds to the generated charge and I_{exc} to the laser fluence. Prior to the application of the rectangular bias voltage, V_{coll}, we find the high-M_n P3HT-based OPV device generates more Q_{pre} across the whole range of laser fluences applied. The smaller amount of charge collected from the low-M_n P3HT-based OPV is attributed to geminate charge recombination losses at short-circuit conditions, evident from the deviation of the power-law exponent α from linearity. Interestingly, after applying the rectangular bias voltage of V_{coll}= -4 Volts the situation is reversed and the largest amount of total collected charge, Q_{tot} is delivered by the low-M_n P3HT-based OPV device. The improved charge extraction efficiency of the low-M_n P3HT-based device in respect to the high-M_n P3HT-based device can be understood because of a photogeneration mechanism that is operative in the presence of the

static external field created by the bias pulse V_{coll}. Considering the thickness of the P3HT:PCBM[60] layers, this electric field has a typical value 40×10^6 V m^{-1}, which is sufficient for fully dissociating the residual geminate charge pairs in the low-M_n P3HT-based system.

Despite the improved charge extraction efficiency of these devices when the static external field is on, charge recombination losses are increased as can be seen in the decreased value of the power-law exponent α. Although the largest Q_{tot} is extracted by the low-M_n P3HT-based device, the sublinear dependence of the obtained Q_{tot} on excitation fluence for this system is enhanced (α=0.72). A similar field-dependence has been observed at low temperatures for contactless samples of P3HT:PCBM[60] blends, and it was attributed to an enhancement in the Coulomb attraction of electron-hole pairs separated by at least 5 nm. [26] At present, the enhanced non-geminate charge recombination is attributed to the increase in the free charge concentration [27] created by the external electric field. Some of the charge carriers are extracted while others are lost due to non-geminate recombination. Given the duration of the applied bias voltage V_{coll}, the onset of these losses is expected at 1 μs after photoexcitation. To a lesser extent, but similarly, the power-law exponent of the high-M_n P3HT-based device drops to α=0.82.

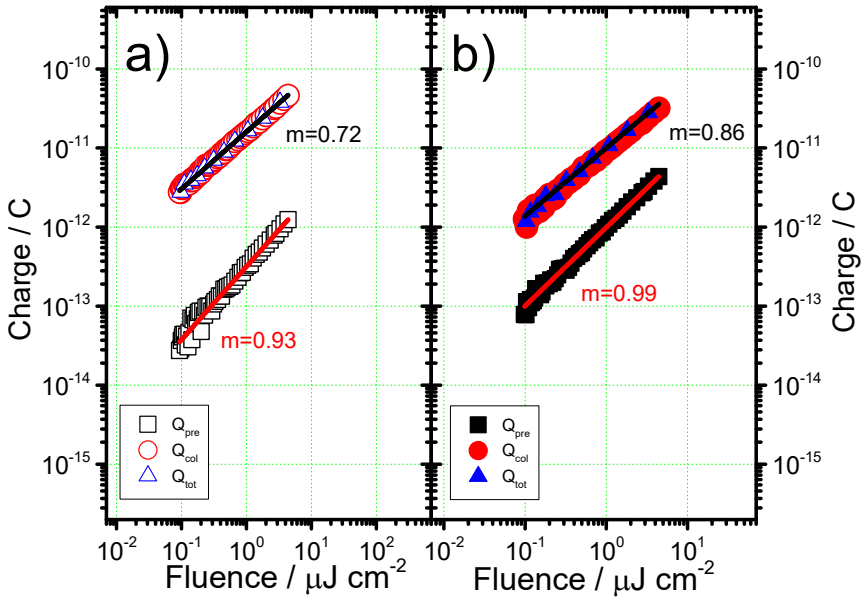

Figure 2. Collected charge as a function of fluence measured with td= 10 ns and V_{pre}= 0 Volts (short-circuit conditions) a) of low-Mn P3HT-PCBM device, and b) of high-Mn P3HT:PCBM[60] device. Both device types were based on annealed P3HT:PCBM[60] layers. The solid lines are linear fits to the data based on the functional form $Q \propto I_{exc}^{\alpha}$ (see text for details).

Next, we addressed the impact of a gradual increase of the applied pre-bias (V_{pre}) on the total amount of collected charge. For this experiment, the 532 nm laser fluence was kept constant at 1 μJ cm^{-2}, t_d was kept fixed at 10 ns, while V_{pre} was varied between -1 – 0.6 Volts. **Figure 3** shows the field dependence of the total extracted charge in the two systems alongside with the associated JV-characteristics of the particular device pixel. Comparing Fig.3a and Fig.3b shows that the total number of generated charges is independent of the field created by V_{pre}, a clear indication of field-independent charge generation. Hence, in both systems the fill factor is predominantly determined by non-geminate recombination losses. In addition, we performed a modified TDCF experiment: both types of OPV devices were photoexcited at 532 nm with a constant fluence of 1 μJ cm^{-2}, while being kept at short-circuit (V_{pre}= 0 Volts), and t_d was varied between V_{pre} and V_{coll}= -4 Volts in the range of 10 – 100 ns. Once again, Fig.3c and Fig.3d demonstrate that despite the lower amount of charge Q_{pre} collected by the low-M_n P3HT-based

device, the amount of total collected charge Q_{tot} is the highest after applying V_{coll} (Fig.3c). In contrast, the amount of total collected charge of the high-M_n P3HT-based device is lower. More importantly, for the high-M_n P3HT-based device the largest fraction of total charge, Q_{pre}, is extracted prior to the application of V_{coll} when the device is kept at short-circuit conditions, as evident by the gradual reduction of the collected charge Q_{coll}, during the application of V_{coll} (Fig.3d).

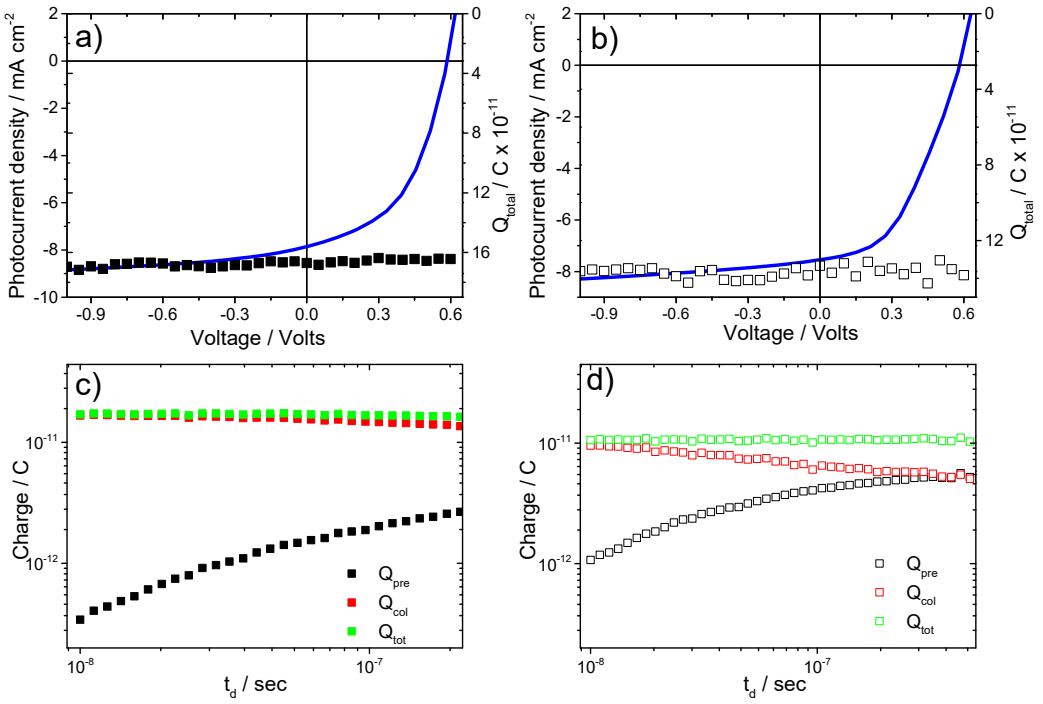

Figure 3. Total amount of charge (Q_{tot}) extracted from the device as a function of applied pre-bias and the corresponding J-V curves of devices prepared with annealed photoactive layers of a) low-M_n P3HT:PCBM[60], b) high-M_n P3HT:PCBM[60]. The amount of charges, Q_{tot}, Q_{col}, and Q_{pre} as a function of delay time extracted from: c) low-M_n P3HT:PCBM[60], and d) high-M_n P3HT:PCBM[60].

Altogether, the results obtained by TDCF suggest that the devices based on the P3HT:PCBM[60] photoactive layers that contain the densely-packed P3HT polymorph, have the capability to facilitate charge carrier collection in the presence of an external electric field, and that the charge collection efficiency in these systems dominates over the antagonistic process of non-geminate charge recombination. This corroborates with the much higher hole

mobility measured in hole-only devices prepared from P3HT with the particular polymorph distribution [19] and it provides a reasonable explanation why the FF determined for the low-M_n P3HT-based device is the highest. However, the exact microscopic mechanism that leads to efficient charge carrier collection in the presence of the densely-packed P3HT polymorphs is unclear. We hypothesize, that this could be related to the lower energetic disorder found in low-M_n P3HT-based blends of P3HT:PCBM[60], which supports a high charge extraction rate. [28]

For a direct comparison of the results obtained by TDCF on device structures with results obtained by all-optical spectroscopy, we performed a set of ultrafast TA experiments on P3HT:PCBM[60] blends that were prepared in an identical manner as the devices' active layers, but deposited on plain quartz substrates. The ps – ns TA spectra of thermally-annealed P3HT:PCBM[60] layers are presented in **Figure 4**; Fig.4a and Fig.4b shows the TA data for the films prepared with the low-M_n and the high-M_n P3HT derivatives, respectively.

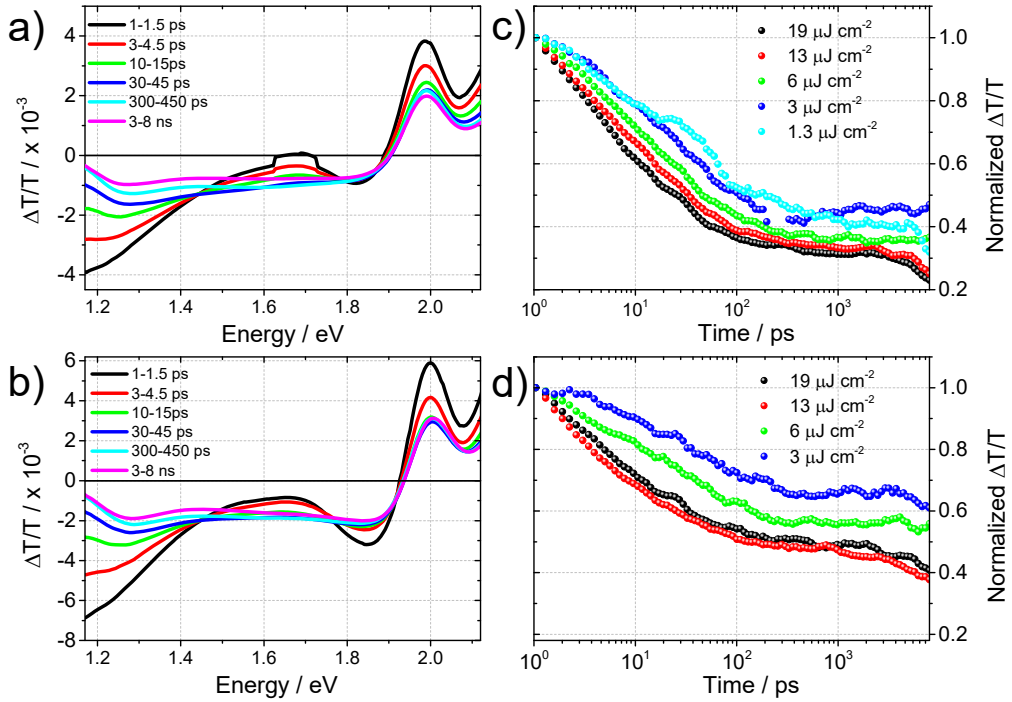

Figure 4. ps – ns transient absorption spectra for annealed P3HT:PCBM[60] blend films developed by a) a low-M_n P3HT derivative and b) high-M_n P3HT derivative. Fluence-dependent kinetics extracted at the region of photoinduced absorption in the spectral range of 1.2 – 1.3 eV for annealed P3HT:PCBM[60] blend films developed by c) a low-M_n P3HT derivative and d) high-M_n P3HT derivative. The TA spectra shown in a) and b) were registered with a fluence of 19 μJ cm^{-2}.

The obtained TA spectra exhibit the characteristic ground state bleach (GSB) of P3HT at 2.0 eV and photo-induced absorption (PA) in the range of 1.2 – 1.4 eV, whilst stimulated emission (SE) of singlet excitons appears between 1.5 – 1.8 eV super-positioned on the PA band, leading to a net negative TA signal. The dynamics of the photogenerated charge carriers can be monitored in the spectral region around 1.2 – 1.3 eV of the PA band. In the TA spectra, an isosbestic point is apparent at 1.45 eV. [29] The SE band can be tracked up to 4 ps, while later on it is masked by the emergence of charge-induced absorption, which co-exists with the exciton-induced absorption up to 30 ps after photoexcitation. Considering the previously reported exciton diffusion coefficient of crystalline P3HT is $D = 1.8\times10^{-3} – 7.9\times10^{-3}$ cm^2 s^{-1}, [30] from the lifetime of the SE signal we deduce that P3HT excitons can probe a distance of 2.3 – 4.8 nm

of P3HT domains in the P3HT:PCBM[60] blends. This is consistent with the high-resolution AFM images shown in Fig. 1 and also with previous ultrafast TA studies [31] that showed concomitant charge photogeneration and exciton diffusion in P3HT:PCBM[60] blend films on the ps timescale. At later times, the remaining PA band is exclusively from charges. A direct comparison between the two systems does not provide any distinct differences with respect to the evolution of the TA spectra. Differences though can be identified in the charge carrier dynamics. The extracted TA kinetics of the photogenerated charge carriers in the two sets of samples are displayed in Fig.4c and Fig.4d, respectively for a range of different photoexcitation intensities. Clearly, in both types of blends the decay dynamics accelerate at high photoexcitation fluences, suggesting the presence of higher order processes occurring at early delay times, *i.e.* exciton-charge or exciton-exciton annihilation. For all fluences, the TA kinetics are found to be considerably faster when the low-M_n P3HT derivative is used. The sole contribution of charges in the TA dynamics can be identified when the TA signal decay is monitored at the isosbestic point (Figure S5; at the lowest fluence, monomolecular recombination prevails, whilst at higher fluences the occurrence of non-geminate charge recombination is seen). This complements the information collected from the TDCF experiments that also identified the onset of severe non-geminate charge recombination losses in the device structure prepared with the low-M_n P3HT derivative.

To further investigate the recombination dynamics of long-lived charge carriers, TA measurements covering the time range up to 300 μs were performed. The data are shown in **Figure 5**. Fig.5a and Fig.5b present the TA spectra recorded for the low-M_n and the high-M_n P3HT-based P3HT:PCBM[60] blend films, respectively. Once again, the evolution of the ns – μs TA spectra demonstrates qualitatively that non-geminate recombination is faster in the case of the low-M_n P3HT-based blend film.

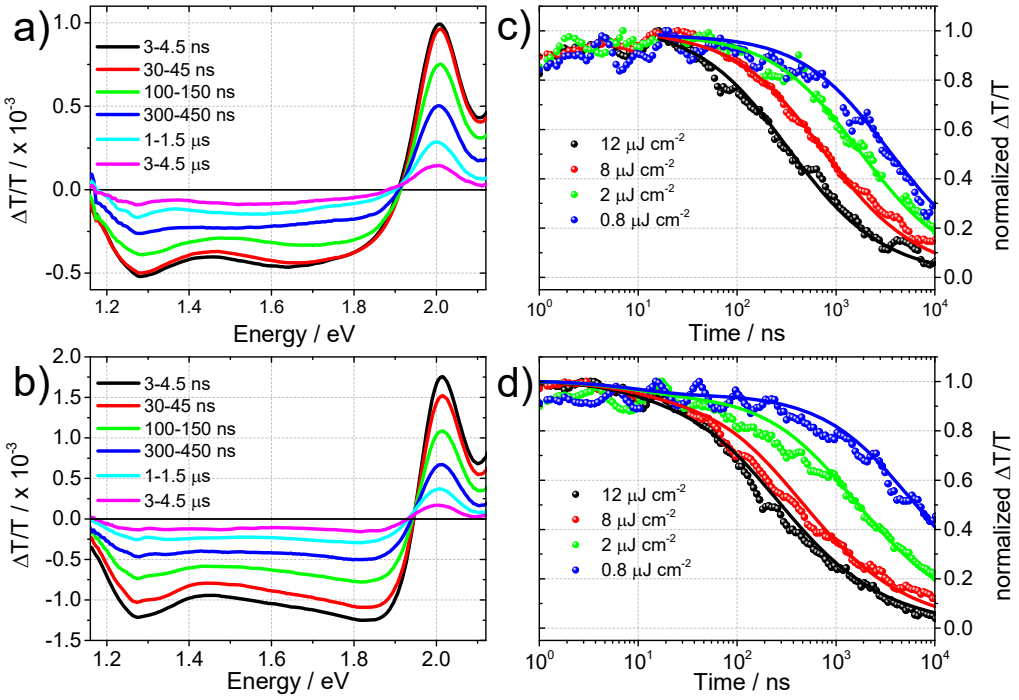

Figure 5. ns – µs transient absorption spectra for annealed P3HT:PCBM[60] blend films developed by a) a low-M_n P3HT derivative and b) a high-M_n P3HT derivative. Fluence-dependent kinetics of photoinduced absorption monitored in the spectral range of 1.2-1.3 eV for P3HT:PCB M[60] blend films developed by c) a low-M_n P3HT derivative and d) high-M_n P3HT derivative. The TA spectra shown in a) and b) were registered with a fluence of 12 µJ cm^{-2}. In both c) and d), the solid lines correspond to fits of the two-pool model of charge recombination (see text and Table 3 for further details).

To quantify the process of charge recombination, the fluence dependence of the charge carrier dynamics was fitted by a two-pool model (see Fig.5c and Fig.5d) as previously used to fit the carrier recombination in different OPV blends.[29] The fit allows to determine the fraction *f* of free charge generation, 1-*f* corresponding to the fraction of charge-transfer states, *k* the geminate recombination rate, $\lambda+1$ the non-geminate recombination order, and γ the non-geminate recombination coefficient. We note that in donor-acceptor bulk heterojunction blend films non-geminate recombination is discussed in the framework of Langevin-type recombination, that is, the nongeminate recombination coefficient depends on the charge carrier mobilities of holes and electrons. However, typically a dimensionless reduction factor

ξ is required, since the experimentally observed recombination coefficients are significantly smaller than those predicted by the Langevin model. This is a consequence of the bulk heterojunction morphology, [32] which allows charge recombination only at the donor-acceptor interface. In this respect, high carrier mobilities increase the nongeminate recombination rate, but are not detrimental to the device performance as they facilitate extraction of free charges prior to nongeminate recombination. In fact, it is the morphology and energetic landscape, which controls the magnitude of the reduction factor and thus careful control of both allows optimum carrier collection, limiting nongeminate recombination.

The fit parameters extracted by the two-pool model were used to calculate an 'effective (bimolecular) recombination coefficient' for the two systems for a carrier density approximately equivalent to one sun (100 mW cm^{-2}). The calculated values for the effective recombination coefficient β are determined to 1.2×10^{-12} cm^3 s^{-1} and 5.2×10^{-13} cm^3 s^{-1} for the low-M_n and high-M_n P3HT-based P3HT:PCBM[60] blend films, respectively. Table 3 summarizes the fit parameters obtained from the two-pool model for the two systems studied.

Parameter	Low-M_n P3HT:PCBM[60]	High-M_n P3HT:PCBM[60]
f	0.98 ± 0.01	0.95 ± 0.001
$1\text{-}f$	0.02	0.05
k / s^{-1}	$1.9\times10^{8} \pm 3.1\times10^{6}$	$1.0\times10^{8} \pm 1.7\times10^{6}$
$\lambda+1$	2.28 ± 0.01	2.50 ± 0.01
γ $(cm^3)^{\lambda}sec^{-1}$	$6.8\times10^{-17} \pm 1.3\times10^{-18}$	$7.3\times10^{-21} \pm 3.6\times10^{-21}$
β / cm^3sec^{-1}	1.2×10^{-12}	5.2×10^{-13}

Table 3. Fit parameters obtained from the two-pool model fit describing the ns – μs charge carrier recombination dynamics in annealed P3HT:PCBM[60] blends with different P3HT polymorph content (see text for details). All parameters were extracted based on carrier densities of 8.75×10^{16} cm^{-3}, 2.11×10^{17} cm^{-3}, 5.80×10^{17} cm^{-3} and 6.90×10^{17} cm^{-3} for the samples made of high-M_n P3HT, and of 4.30×10^{16} cm^{-3}, 1.10×10^{17} cm^{-3}, 1.90×10^{17} cm^{-3} and 4.80×10^{17} cm^{-3} for the samples made of the low-M_n P3HT.

Figure 6 presents diagrammatically the relationship between the P3HT polymorph distribution of the P3HT:PCBM[60] blend films and the experimentally observable quantities.

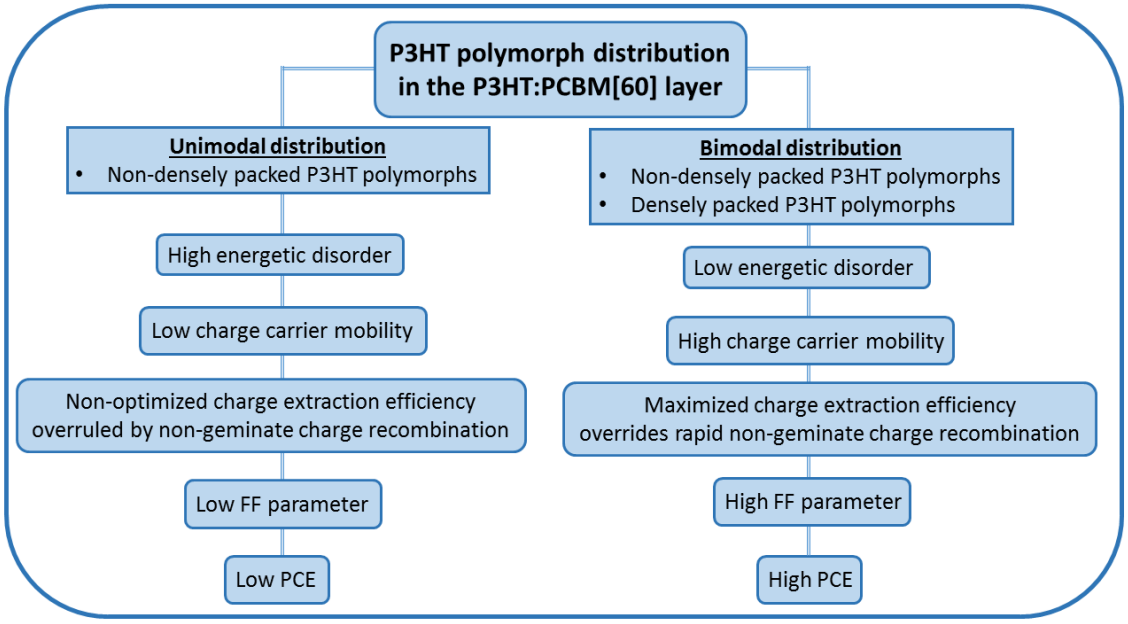

Figure 6. The impact of P3HT polymorphism present in the P3HT:PCBM[60] blends on the antagonistic correlation between charge extraction and non-geminate charge recombination, and the overall effect of different P3HT polymorph distributions on device performance.

It is plausible that the higher fraction of free charge generation *f* that is found for the low-M_n P3HT-based blend films is due to the co-existence of densely-packed and non-densely-packed polymorphs. The formation of additional interface area between domains of different degrees of order [33] may provide a larger active surface area for exciton dissociation. In agreement with the TDCF results and in line with the findings from the ps-ns TA measurements, the presence of densely-packed P3HT polymorphs in the P3HT:PCBM[60] blends prepared by the low-M_n P3HT batch result in a twofold larger effective bimolecular recombination rate with respect to the blend films based on the high-M_n P3HT derivative.

Conclusions

In conclusion, the combination of two transient spectroscopic techniques unveils the impact of densely-packed P3HT polymorphs in P3HT:PCBM[60] blends on the overall PCE of their

corresponding OPV devices. When densely-packed P3HT polymorphs are present in the P3HT:PCBM[60] blend, the charge carrier extraction efficiency is the highest, effectively overruling the losses by non-geminate charge recombination, and enabling a maximum FF and device performance. In the absence of densely-packed polymorphs (high-M_n P3HT-based P3HT:PCBM[60]), non-geminate recombination losses are less pronounced, however, the efficiency of charge carrier extraction in the operating OPV device is lower. Raman spectroscopy provides further information concerning the effect of the densely-packed P3HT polymorphs on the optimized charge carrier extraction, as it suggests minimal energetic disorder in the low-M_n P3HT:PCBM[60] blends after annealing. Overall, our study provides insight into the impact of polymorphism on the antagonistic processes of charge carrier extraction and non-geminate charge recombination losses in solution-processed OPV composite films. The knowledge gained by these results can be useful in the optimization of different types of optoelectronic devices, *e.g.* fullerene-free OPV [34, 35] and organic light-emitting diode (OLED) devices. [36] The impact of polymorphism on charge carrier mobility should be taken into consideration when different material polymorphs are selected for tuning the spectral response of OLED devices. Likewise, the performance-limiting effects of increased energetic disorder in OPV layers developed by non-fullerene electron acceptors could be minimized if the broad distribution of structural packing motifs of the electron acceptor moiety is adjusted.

ASSOCIATED CONTENT

Supporting Information. Methods, overview of Raman results, schematic of the time-delayed-collection field experiment, fluence-dependent charge carrier dynamics monitored at the isosbestic point. The following file is available free of charge: Supporting Information_manuscript.pdf

AUTHOR INFORMATION

Panagiotis E. Keivanidis, Frédéric Laquai

Notes

The authors declare no competing financial interests.

ACKNOWLEDGMENT

The research reported in this publication was supported by funding from King Abdullah University of Science and Technology (KAUST). P.E.K acknowledges the support of a start-up fund provided by the Cyprus University of Technology. E. L. and S. C. H. would like to acknowledge the support from the European Union's Horizon 2020 research and innovation program under the Marie Sklodowska-Curie grant agreement No 675867.

REFERENCES

1. Brabec, C. J.; Gowrisanker, S.; Halls, J. J. M.; Laird, D.; Jia, S.; Williams, S. P. Polymer–Fullerene Bulk-Heterojunction Solar Cells. *Adv. Mater.* **2010,** *22*, 3839-3856.

2. Søndergaard, R.; Hösel, M.; Angmo, D.; Larsen-Olsen, T. T.; Krebs, F. C. Roll-to-roll Fabrication of Polymer Solar Cells. *Mater. Today* **2012,** *15*, 36-49.

3. Gasparini, N.; Lucera, L.; Salvador, M.; Prosa, M.; Spyropoulos, G. D.; Kubis, P.; Egelhaaf, H.-J.; Brabec, C. J.; Ameri, T. High-performance Ternary Organic Solar Cells with Thick Active Layer Exceeding 11% Efficiency. *Energy Environ. Sci.* **2017,** *10*, 885-892.

4. Nelson, J. Polymer:Fullerene Bulk Heterojunction Solar Cells. *Mater. Today* **2011,** *14*, 462-470.

5. Scharber, M. C.; Sariciftci, N. S. Efficiency of Bulk-Heterojunction Organic Solar Cells. *Prog. Polym. Sci.* **2013,** *38*, 1929-1940.

6. Clarke, T. M.; Durrant, J. R. Charge Photogeneration in Organic Solar Cells. *Chem. Rev.* **2010,** *110*, 6736-6767.

7. Vithanage, D. A.; Devižis, A.; Abramavičius, V.; Infahsaeng, Y.; Abramavičius, D.; MacKenzie, R. C. I.; Keivanidis, P. E.; Yartsev, A.; Hertel, D.; Nelson, J. et al. Visualizing Charge Separation in Bulk Heterojunction Organic Solar Cells. *Nat. Commun.* **2013,** *4*, 2334.

8. Gélinas, S.; Rao, A.; Kumar, A.; Smith, S. L.; Chin, A. W.; Clark, J.; van der Poll, T. S.; Bazan, G. C.; Friend, R. H. Ultrafast Long-Range Charge Separation in Organic Semiconductor Photovoltaic Diodes. *Science* **2014,** *343*, 512-516.

9. Bartesaghi, D.; Pérez, I. d. C.; Kniepert, J.; Roland, S.; Turbiez, M.; Neher, D.; Koster, L. J. A. Competition Between Recombination and Extraction of Free Charges Determines the Fill Factor of Organic Solar Cells. *Nat. Commun.* **2015,** *6*, 7083.

10. Kim, Y.; Choulis, S. A.; Nelson, J.; Bradley, D. D. C.; Cook, S.; Durrant, J. R. Composition and Annealing Effects in Polythiophene/Fullerene Solar Cells. *J. Mater. Sci.* **2005,** *40*, 1371-1376.

11. Wadsworth, A.; Hamid, Z.; Bidwell, M.; Ashraf, R. S.; Khan, J. I.; Anjum, D. H.; Cendra, C.; Yan, J.; Rezasoltani, E.; Guilbert, A. A. Y. et al. Progress in Poly (3-Hexylthiophene) Organic Solar Cells and the Influence of its Molecular Weight on Device Performance. *Adv. Energy Mater.* **2018,** *8*, 1801001

12. Baek, W.-H.; Yoon, T.-S.; Lee, H. H.; Kim, Y.-S. Composition-Dependent Phase Separation of P3HT:PCBM Composites for High Performance Organic Solar Cells. *Org. Electron.* **2010,** *11*, 933-937.

13. van Franeker, J. J.; Turbiez, M.; Li, W.; Wienk, M. M.; Janssen, R. A. J. A Real-Time Study of the Benefits of co-Solvents in Polymer Solar Cell Processing. *Nat. Commun.* **2015,** *6*, 6229.

14. Kniepert, J.; Lange, I.; Heidbrink, J.; Kurpiers, J.; Brenner, T. J. K.; Koster, L. J. A.; Neher, D. Effect of Solvent Additive on Generation, Recombination, and Extraction in PTB7:PCBM Solar Cells: A Conclusive Experimental and Numerical Simulation Study. *J. Mater. Chem. C* **2015,** *119*, 8310-8320.

15. Poelking, C.; Andrienko, D. Effect of Polymorphism, Regioregularity and Paracrystallinity on Charge Transport in Poly(3-hexylthiophene) [P3HT] Nanofibers. *Macromolecules* **2013,** *46*, 8941-8956.

16. Zhugayevych, A.; Mazaleva, O.; Naumov, A.; Tretiak, S. Lowest-Energy Crystalline Polymorphs of P3HT. *J. Mater. Chem. C* **2018,** *122*, 9141-9151.

17. Panzer, F.; Sommer, M.; Bässler, H.; Thelakkat, M.; Köhler, A. Spectroscopic Signature of Two Distinct H-Aggregate Species in Poly(3-hexylthiophene). *Macromolecules* **2015**, *48*, 1543-1553.

18. Dang, M. T.; Hirsch, L.; Wantz, G. P3HT:PCBM, Best Seller in Polymer Photovoltaic Research. *Adv. Mater.* **2011,** *23*, 3597-3602.

19. Kan, Z.; Colella, L.; Canesi, E. V.; Vorobiev, A.; Skrypnychuk, V.; Terraneo, G.; Barbero, D. R.; Bertarelli, C.; MacKenzie, R. C. I.; Keivanidis, P. E. Charge Transport Control via Polymer Polymorph Modulation in Ternary Organic Photovoltaic Composites. *J. Mater. Chem. A* **2016,** *4*, 1195-1201.

20. Kurpiers, J.; Neher, D. Dispersive Non-Geminate Recombination in an Amorphous Polymer:Fullerene Blend. *Sci. Rep.* **2016,** *6*, 26832.

21. Razzell-Hollis, J.; Limbu, S.; Kim, J.-S. Spectroscopic Investigations of Three-Phase Morphology Evolution in Polymer:Fullerene Solar Cell Blends. *J. Phys. Chem. C* **2016,** *120*, 10806-10814.

22. Razzell-Hollis, J.; Tsoi, W. C.; Kim, J.-S. Directly Probing The Molecular Order of Conjugated Polymer in OPV Blends Induced by Different Film Thicknesses, Substrates and Additives. *J. Mater. Chem. C* **2013,** *1*, 6235-6243.

23. Campoy-Quiles, M.; Ferenczi, T.; Agostinelli, T.; Etchegoin, P. G.; Kim, Y.; Anthopoulos, T. D.; Stavrinou, P. N.; Bradley, D. D. C.; Nelson, J. Morphology Evolution via Self-Organization and Lateral and Vertical Diffusion in Polymer:Fullerene Solar Cell Blends. *Nat. Mater.* **2008,** *7*, 158.

24. Pivrikas, A.; Sariciftci, N. S.; Juška, G.; Österbacka, R. A Review of Charge Transport and Recombination in Polymer/Fullerene Organic Solar Cells. *Prog. Photovoltaics* **2007,** *15*, 677-696.

25. Craciun, N. I.; Wildeman, J.; Blom, P. W. M. Universal Arrhenius Temperature Activated Charge Transport in Diodes from Disordered Organic Semiconductors. *Phys. Rev. Lett.* **2008,** *100*, 056601.

26. Athanasopoulos, S.; Greenham, N. C.; Friend, R. H.; Chepelianskii, A. D. Field-Enhanced Recombination at Low Temperatures in an Organic Photovoltaic Blend. *Phys. Rev. B* **2015,** *92*, 125301.

27. Marsh, R. A.; Groves, C.; Greenham, N. C. A Microscopic Model for the Behavior of Nanostructured Organic Photovoltaic Devices. *J. Appl. Phys.* **2007,** *101*, 083509.

28. Brendan, W.; Yukihiro, N.; M., C. T.; Kouichi, O.; Heikki, P.; J., M. A.; Shogo, M. Quantifying Recombination Losses during Charge Extraction in Bulk Heterojunction Solar Cells Using a Modified Charge Extraction Technique. *Adv. Energy Mater.* **2017,** *7*, 1602026.

29. Howard, I. A.; Mauer, R.; Meister, M.; Laquai, F. Effect of Morphology on Ultrafast Free Carrier Generation in Polythiophene:Fullerene Organic Solar Cells. *J. Am. Chem. Soc.* **2010,** *132*, 14866-14876.

30. Tamai, Y.; Ohkita, H.; Benten, H.; Ito, S. Exciton Diffusion in Conjugated Polymers: From Fundamental Understanding to Improvement in Photovoltaic Conversion Efficiency. *J. Phys. Chem. Lett.* **2015,** *6*, 3417-3428.

31. Kirkpatrick, J.; Keivanidis, P. E.; Bruno, A.; Ma, F.; Haque, S. A.; Yarstev, A.; Sundstrom, V.; Nelson, J. Ultrafast Transient Optical Studies of Charge Pair Generation and Recombination in Poly-3-Hexylthiophene(P3HT):[6,6]Phenyl C61 Butyric Methyl Acid Ester (PCBM) Blend Films. *J. Phys. Chem. B* **2011,** *115*, 15174-15180.

32. Pivrikas, A.; Juška, G.; Mozer, A. J.; Scharber, M.; Arlauskas, K.; Sariciftci, N. S.; Stubb, H.; Österbacka, R. Bimolecular Recombination Coefficient as a Sensitive Testing Parameter for Low-Mobility Solar-Cell Materials. *Phys. Rev. Lett.* **2005,** *94*, 176806.

33. Reid, O. G.; Malik, J. A. N.; Latini, G.; Dayal, S.; Kopidakis, N.; Silva, C.; Stingelin, N.; Rumbles, G. The Influence of Solid-State Microstructure on the Origin and Yield of Long-Lived Photogenerated Charge in Neat Semiconducting Polymers. *J. Polym. Sci., Part B: Polym. Phys.* **2012,** *50*, 2

34. Aluicio-Sarduy, E.; Singh, R.; Kan, Z.; Ye, T.; Baidak, A.; Calloni, A.; Berti, G.; Duò, L.; Iosifidis, A.; Beaupré, S. et al. Elucidating the Impact of Molecular Packing and Device Architecture on the Performance of Nanostructured Perylene Diimide Solar Cells. *ACS Appl. Mater. Interfaces* **2015,** *7*, 8687-8698.

35. Singh, R.; Lee, J.; Kim, M.; Keivanidis, P. E.; Cho K. Control of the Molecular Geometry and Nanoscale Morphology in Perylene Diimide Based Bulk Heterojunctions Enables an Efficient Non-Fullerene Organic Solar Cell, *J. Mater. Chem. A*, **2017**, *5*, 210-220.

36. Hladka, I.; Volyniuk, D.; Bezvikonnyi, O.; Kinzhybalo, V.; Bednarchuk, T. J.; Danyliv, Y.; Lytvyn, R.; Lazauskas, A.; Grazulevicius, J. V. Polymorphism of Derivatives of tert-Butyl Substituted Acridan and Perfluorobiphenyl as Sky-Blue OLED Emitters Exhibiting

Aggregation Induced Thermally Activated Delayed Fluorescence. *J. Mater. Chem. C* **2018**, doi: 10.1039/C8TC04867C.

TOC Graphic

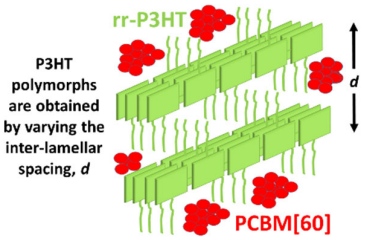
rr-P3HT
P3HT
polymorphs
are obtained
by varying the
inter-lamellar
spacing, d
d
PCBM[60]